

Supporting Information

Highly efficient electrochemical CO₂ reduction over crystalline-amorphous In₂O₃-CeO_x heterostructures

Cuifeng Wang, Zhaohui Wu, Guihao Liu, Sha Bai, Lin Guo, Lei He and Yu-Fei Song**

State Key Laboratory of Chemical Resource Engineering, Beijing University of Chemical Technology, Beijing 100029 P. R. China.

List of contents:

Experimental procedures

Figure S1. Schematic illustration of the synthesis process of In₂O₃-CeO_x.

Figure S2. Corresponding EDX mapping images of In₂O₃-CeO₂.

Figure S3. XPS spectra of a) Ce 3d for CeO₂ and b) In₂O₃-CeO₂. c) LSVs of In₂O₃ and In₂O₃-CeO₂ in CO₂-saturated 0.5 M KHCO₃ at a scan rate of 50 mV s⁻¹.

Figure S4. The CV curve of a) In₂O₃-CeO_x and b) carbon paper without any catalyst in CO₂-saturated 0.5 M KHCO₃ at a scan rate of 50 mV s⁻¹.

Figure S5. a) LSV curves of In₂O₃-CeO_x, In₂O₃-CeO₂ and In₂O₃ electrode in Ar-saturated electrolyte at a scan rate of 50 mV s⁻¹.

Figure S6. NMR spectrum of the liquid products for In₂O₃-CeO_x after electrolysis at -0.9 V in CO₂-saturated 0.5 M KHCO₃.

Figure S7. The FE_{Formate}, FE_{CO} and FE_{H₂} of a) In₂O₃-CeO_x, b) In₂O₃-CeO₂ at different applied potentials respectively. The FE_{H₂} of c) CeO_x, d) CeO₂ at different applied potentials respectively.

Figure S8. The LSV curve of the In₂O₃-CeO_x before and after stability test at -0.9V.

Figure S9. a-b) HRTEM and c-f) elemental mapping of the In₂O₃-CeO_x after 20 h stability test.

Figure S10. Cyclic voltammograms of a) In₂O₃-CeO_x, b) In₂O₃-CeO₂ and c) In₂O₃ between -0.55V and -0.50 V vs. RHE in CO₂-saturated 0.5 M KHCO₃.

Figure S11. The normalized current density for formate production by ECSA for In₂O₃-CeO_x, In₂O₃-CeO₂ and In₂O₃.

Figure S12. a, b, c) Mott-Schottky plots of In₂O₃, CeO_x and CeO₂ respectively. d) valance band XPS spectra.

Figure S13. Schematic illustration for charge transfer in In₂O₃-CeO₂.

Figure S14. The catalytic pathway on In₂O₃-CeO_x based on the *OCHO and *HCOOH adsorption intermediates after optimization. Purple, yellow, red, brown, white spheres represent In, Ce, O, C, and H atoms, respectively.

Figure S15. The computational structure and adsorption models In₂O₃-CeO₂ after optimization. a) In₂O₃-CeO₂, b) *CO₂ on In₂O₃-CeO₂, c) *OCHO on In₂O₃-CeO₂, d) *HCOOH on In₂O₃-CeO₂. Purple, yellow, red, brown, white spheres represent In, Ce, O, C, and H atoms, respectively.

Figure S16. The computational structure and adsorption models In₂O₃ after optimization. a) In₂O₃, b) *CO₂ on In₂O₃, c) *OCHO on In₂O₃, d) *HCOOH on In₂O₃. Purple, yellow, red,

brown, white spheres represent In, Ce, O, C, and H atoms, respectively.

Table 1. Comparison of the highest FE and potential on some reported In-based electrocatalysts for the electrochemical reduction of CO₂ to formate.

References

Experimental Procedures

Chemicals: Cerium (III) nitrate hexahydrate ($\text{Ce}(\text{NO}_3)_3 \cdot 6\text{H}_2\text{O}$, Aladdin Reagent Co., Ltd), sodium hydroxide (NaOH, Aladdin Reagent Co., Ltd), sodium borohydride (NaBH_4 , Aladdin Reagent Co., Ltd), indium (III) chloride tetrachloride ($\text{InCl}_3 \cdot 4\text{H}_2\text{O}$, Aladdin Reagent Co., Ltd), indium oxide (In_2O_3 , Energy Chemical), sodium carbonate (Na_2CO_3 , FuChen Chemical Reagent Co., Ltd), sodium sulfate anhydrous (K_2SO_4 , FuChen Chemical Reagent Co., Ltd), ethanol ($\text{C}_2\text{H}_5\text{OH}$, 99.7%, FuYu Chemical Works.), Nafion-117 membrane (Alfa Aesar China Co., Ltd), CO_2 (99.999 %, North Temperature Gas Factory). All the chemicals were used without further purification. The deionized water used in all experiments was with a specific resistance of $18.2 \text{ M}\Omega \cdot \text{cm}$.

Materials Preparation:

Synthesis of CeO_x . CeO_x was synthesized through a one-step reduction. Typically, $\text{Ce}(\text{NO}_3)_3 \cdot 6\text{H}_2\text{O}$ (1.7 g) was dissolved in H_2O (20 mL) and stirred until transparent solution, and then NaBH_4 (400 mg) was added and stirred intensely (20 min). After that, the mixture was washed several times by deionized water. Ultimately, CeO_x was dried at 60°C overnight.

Synthesis of CeO_2 . CeO_2 was prepared using a solvothermal treatment. Specifically, $\text{Ce}(\text{NO}_3)_3 \cdot 6\text{H}_2\text{O}$ (0.8 g) was put into H_2O (5mL), and then the mixture was added into NaOH (6M, 35 mL) and stirred intensely (30 min). After that, the solution was hydrothermal treated at 100°C for 24 h. The final product was washed for several times and dried overnight.

Synthesis of $\text{In}_2\text{O}_3\text{-CeO}_x$. CeO_x (300 mg) was dispersed in H_2O (20 mL) to form a stable solution by ultrasonication and stirring, mixed with $\text{InCl}_3 \cdot 4\text{H}_2\text{O}$ (600 mg) and then ultrasonicated (20 min). Subsequently, Na_2CO_3 (800 mg) was added in H_2O (10 mL), and then the solution was added dropwise under stirring. The mixture was stirred for another 1 h. The precipitate was washed and dried in vacuum at 40°C . Finally, $\text{In}_2\text{O}_3\text{-CeO}_x$ was obtained after the precipitate was heated in a furnace at 300°C for 1h ($5^\circ\text{C} \cdot \text{min}^{-1}$) under an Ar/ H_2 flow.

Synthesis of $\text{In}_2\text{O}_3\text{-CeO}_2$. Except for the initial addition of the as-prepared CeO_2 (300

mg), the remaining steps were consistent with In₂O₃-CeO₂. And In₂O purchased from Energy Chemical.

Characterization: X-ray diffraction (XRD) patterns were characterized by a Rigaku XRD-6000 diffractometer equipped with a Cu K α radiation ($\lambda = 1.5405 \text{ \AA}$). Scanning electron microscopy (SEM) images and energy dispersive X-ray (EDX) analytical data were obtained on the Zeiss Supra 55 SEM equipped with an EDX detector. High-resolution transmission electron microscopy (HR-TEM) images were obtained on a JEOL JEM-2010 transmission electron microscope operating at an acceleration voltage of 200 kV. X-ray photoelectron spectroscopy (XPS) measurements were performed with monochromatized AlK α exciting X-radiation (PHI Quantera SXM).

Electrochemical Measurement:

In general, the electroreduction of CO₂ were carried out by using a H-type cell with three-electrode system. The catalysts were loaded onto carbon paper to serve as the working electrode. Regularly, 5 mg of pre-catalysts (In₂O₃-CeO_x, In₂O₃-CeO_x, and In₂O₃) and 2 mg of acetylene black were dispersing in the mixture of 1ml μ L ethanol, and then 20 μ L of Nafion was added and sonicated for 40 min to achieve uniform solution. Ultimately, the solution was added to carbon paper dropwise and dried.

All the electrochemical experiments were conducted on the electrochemical workstation (CHI 660E). The electrolysis experiments were conducted at 25 °C in a H-type cell with a working cathode, a counter anode (platinum gauze), and a reference electrode Ag/Ag⁺. In the experiment, Nafion-117 membrane was used as the proton exchange membrane that separated the cathode and anode compartments. 0.5 M KHCO₃ solution was utilized as cathodic electrolyte. H⁺ can be transferred from anode compartment to cathode compartment through Nafion-117 membrane, which is the proton source. Before starting the electrolysis experiment, the catholyte was bubbled with CO₂ for 30 min under stirring and the electrolysis was carried out under a steady stream of CO₂. Linear sweep voltammetry (LSV) measurements were performed in Ar or CO₂-bubbled 0.5 M KHCO₃ solution. CO₂ was delivered during the whole CO₂ electrolysis (20 mL·min⁻¹).

Product analysis:

The gaseous product of electrochemical experiments was collected using a gas bag and analyzed by gas chromatography (GC, 2014C), which was equipped with FID and TCD detectors using helium as the internal standard. The liquid product was analyzed by ^1H NMR (Bruker Avance III 400 HD spectrometer) in D_2O with phenol as an internal standard.^[1,2]

Calculation method:

$$FE = \frac{anF}{Q}$$

α : electrons transferred to produce formate ($\alpha = 2$), n : amount of formate produced, F : Faraday constant, Q : total charge consumed during the whole electrolysis.

$$ECSA = RS = \frac{C_{dl}}{Cs}$$

S : the geometric area of work electrode, which is 1 cm^2 in this work, R : the roughness factor, C_{dl} : the double-layer capacitance of work electrode. The specific capacitance (C_s) for a flat surface is generally found to be in the range of $20\text{-}60 \mu\text{F cm}^{-2}$. Based on the literature report,^[3] we adopt $40 \mu\text{F cm}^{-2}$ as the one for calculations of the electrochemically active surface area below.

$$A_{ECSA}^{In_2O_3-CeO_x} = \frac{0.55 \text{ mF cm}^{-2}}{40 \mu\text{F cm}^{-2} \text{ per cm}_{ECSA}^2} = 13.75 \text{ cm}_{ECSA}^2$$

$$A_{ECSA}^{In_2O_3-CeO_2} = \frac{0.46 \text{ mF cm}^{-2}}{40 \mu\text{F cm}^{-2} \text{ per cm}_{ECSA}^2} = 11.50 \text{ cm}_{ECSA}^2$$

$$A_{ECSA}^{In_2O_3} = \frac{0.38 \text{ mF cm}^{-2}}{40 \mu\text{F cm}^{-2} \text{ per cm}_{ECSA}^2} = 9.50 \text{ cm}_{ECSA}^2$$

Density functional theory (DFT) calculations:

Calculations were performed using the DFT method in the CP2K package^[4]. The exchange-correlation potential was described by generalized gradient approximation (GGA) with the spin-polarized Perdew-Burke-Ernzerhof (PBE) functional. Wavefunctions were expanded in molecularly optimized (MOLOPT)^[5] triple ζ -valence polarized basis set with an auxiliary plane-wave basis set with a cutoff energy of 500 Ry. Core electrons were modeled by scalar relativistic norm-conserving Goedecker-

Teter-Hutter (GTH) pseudopotentials^[6] with 12,13, 4, 6, and 1 valence electrons for Ce, In, C, O, and H, respectively. The Ce basis set and pseudopotential were modified to properly account for localized 4f electronic state^[7,8]. DFT + U method was employed to provide a satisfying description of the electronic structure since the strong correlation of 4f electron in Ce, U value of 7.0 eV was used for the Ce^[9]. Grimme's D3(BJ) method^[10,11] was added to study the impact of van der Waals interaction. Only Γ point was used in all calculations. To simulate the surface environment, The atoms in the bottom layer were constrained.

The Gibbs free energy was computed following the equation:

$$\Delta G = \Delta E - T\Delta S + ZPE + \int C_p dT$$

where the ΔE is the electronic energy, ΔS is the entropy, ZPE is the zero-point vibration energy, and the C_p is the heat capacity at $p = 1$ atm and $T = 298.15$ K. These data were obtained by the Shermo program. The ΔE was computed following the equation:

$$\Delta E = E(\text{Slab} + \text{adsorbate}) - E(\text{Slab}) - E(\text{adsorbate})$$

where $E(\text{Slab} + \text{adsorbate})$, $E(\text{Slab})$, and $E(\text{adsorbate})$ are the total energies of the slab with adsorbate, clean slab surface, and adsorbate in the gas phase, respectively.

The projected density of states (p-DOS) was analyzed using the molder file formed in the single-point calculation of the optimized structure of $\text{In}_2\text{O}_3\text{-CeO}_x$ and $\text{In}_2\text{O}_3\text{-CeO}_2$ with the Multiwfn package.^[12] The p-DOS was calculated with the C-Squared Population Analysis (SCPA) method^[13] and the Gaussian function was selected to be the broadening function. The electron density difference and charge displacement curve were analyzed using the cube file formed in the single-point calculation of the optimized structure of $\text{In}_2\text{O}_3\text{-CeO}_x$ and $\text{In}_2\text{O}_3\text{-CeO}_2$ with the Multiwfn package.

Supplementary Figures/Tables

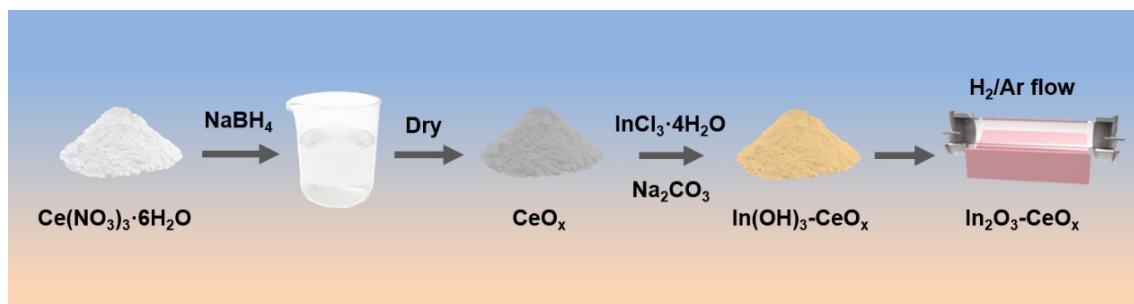


Figure S1. Schematic illustration of the synthesis process of $\text{In}_2\text{O}_3\text{-CeO}_x$.

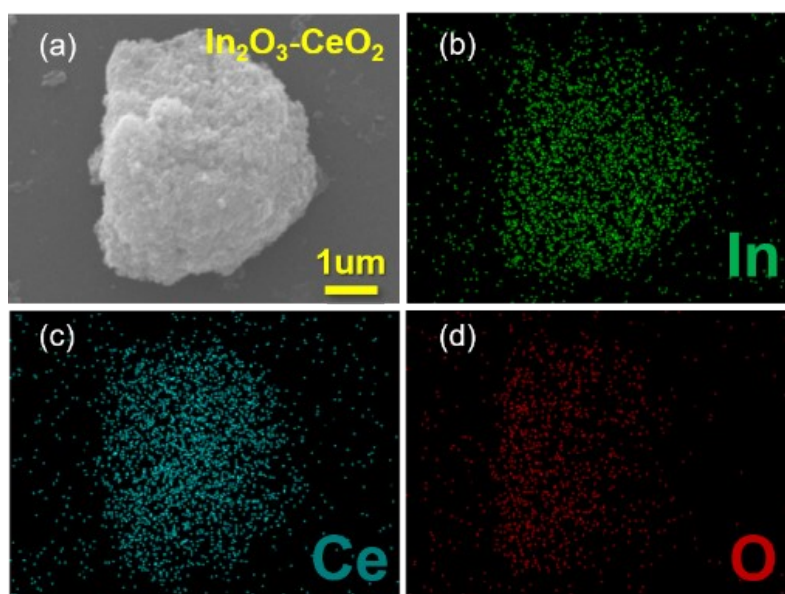


Figure S2. Corresponding EDX mapping images of $\text{In}_2\text{O}_3\text{-CeO}_2$.

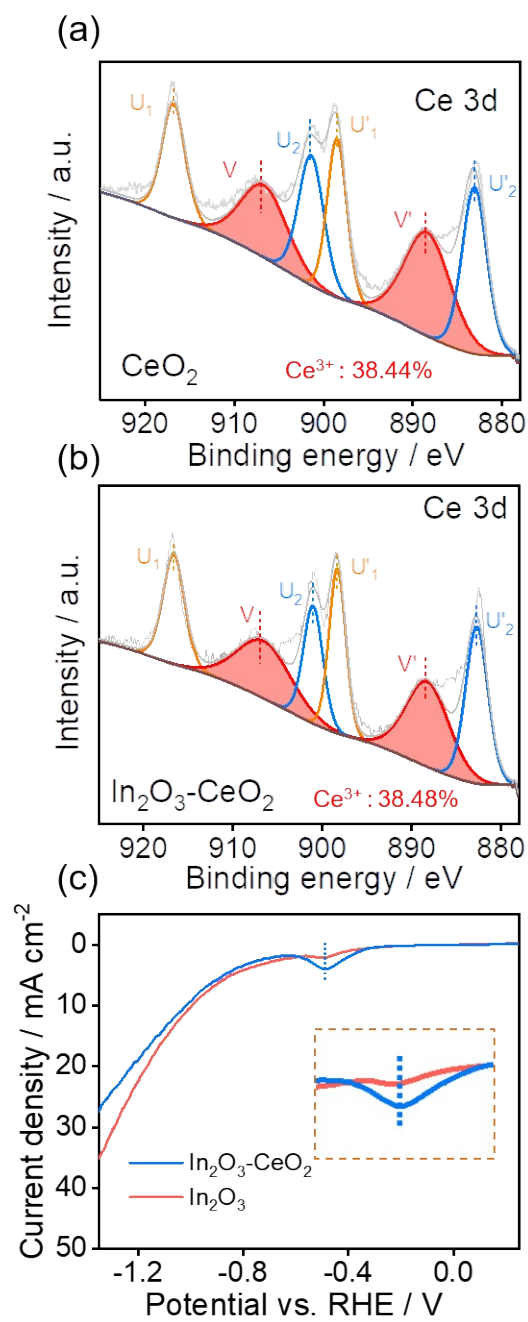


Figure S3. XPS spectra of a) Ce 3d for CeO₂ and b) In₂O₃-CeO₂. c) LSVs of In₂O₃ and In₂O₃-CeO₂ in CO₂-saturated 0.5 M KHCO₃ at a scan rate of 50 mV s⁻¹.

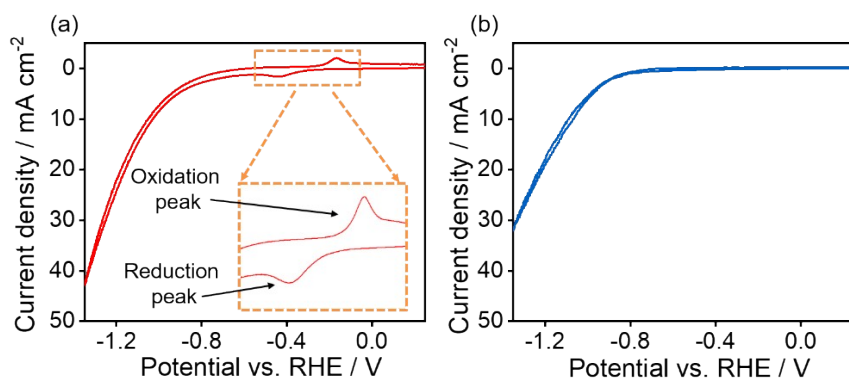


Figure S4. The CV curve of a) $\text{In}_2\text{O}_3\text{-CeO}_x$ and b) carbon paper without any catalyst in CO_2 -saturated 0.5 M KHCO_3 at a scan rate of 50 mV s^{-1} .

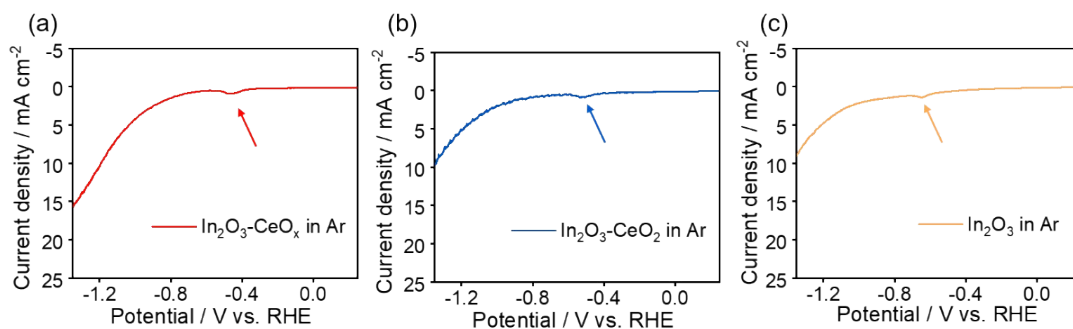


Figure S5. a) LSV curves of $\text{In}_2\text{O}_3\text{-CeO}_x$, $\text{In}_2\text{O}_3\text{-CeO}_2$ and In_2O_3 electrode in Ar-saturated electrolyte at a scan rate of 50 mV s^{-1} .

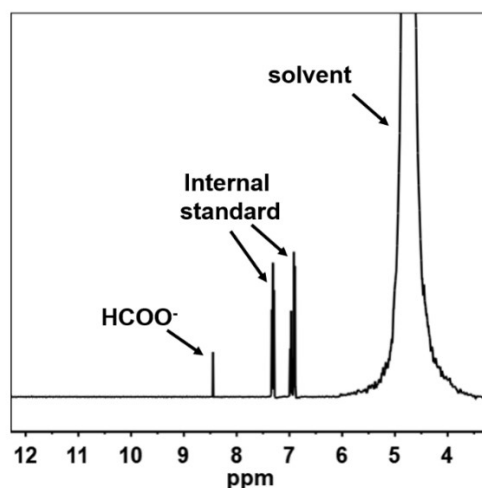


Figure S6. NMR spectrum of the liquid products for $\text{In}_2\text{O}_3\text{-CeO}_x$ after electrolysis at -0.9 V in CO_2 -saturated 0.5 M KHCO_3 .

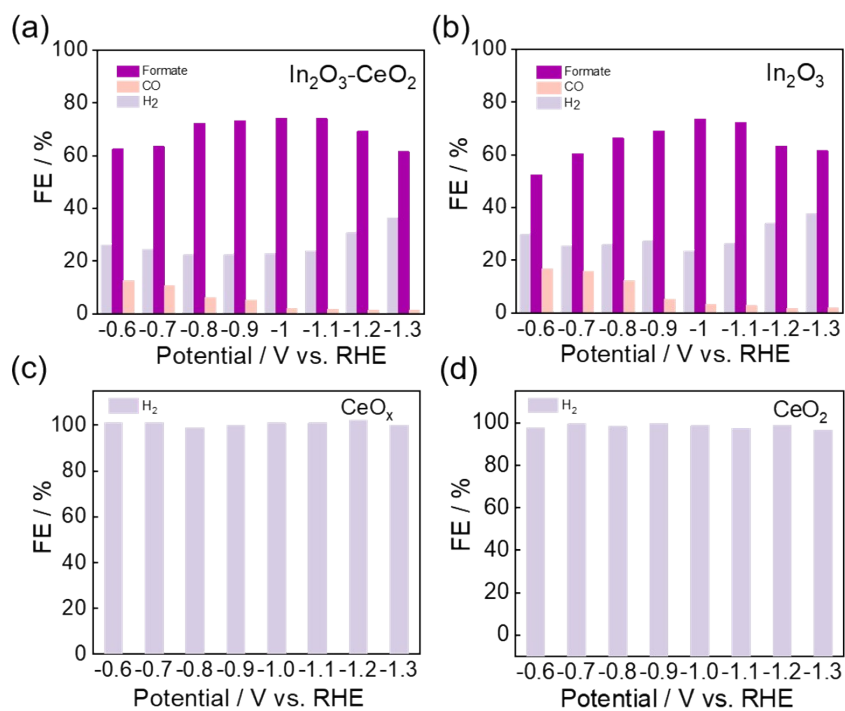


Figure S7. The $\text{FE}_{\text{Formate}}$, FE_{CO} and FE_{H_2} of a) $\text{In}_2\text{O}_3\text{-CeO}_x$, b) $\text{In}_2\text{O}_3\text{-CeO}_2$ at different applied potentials respectively. The FE_{H_2} of c) CeO_x , d) CeO_2 at different applied potentials respectively.

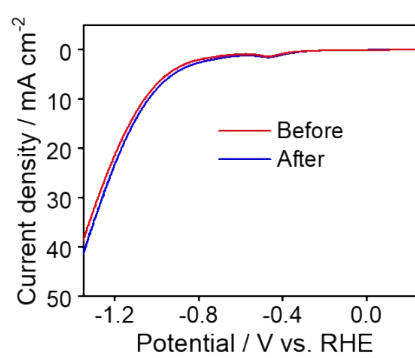


Figure S8. The LSV curve of the $\text{In}_2\text{O}_3\text{-CeO}_x$ before and after stability test at -0.9V .

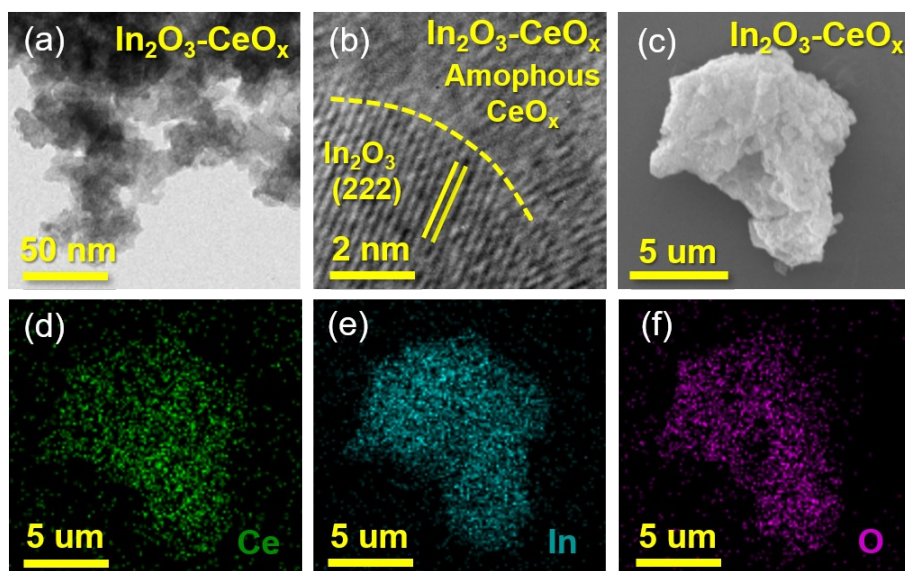


Figure S9. a-b) HRTEM and c-f) elemental mapping of the $\text{In}_2\text{O}_3\text{-CeO}_x$ after 20 h stability test.

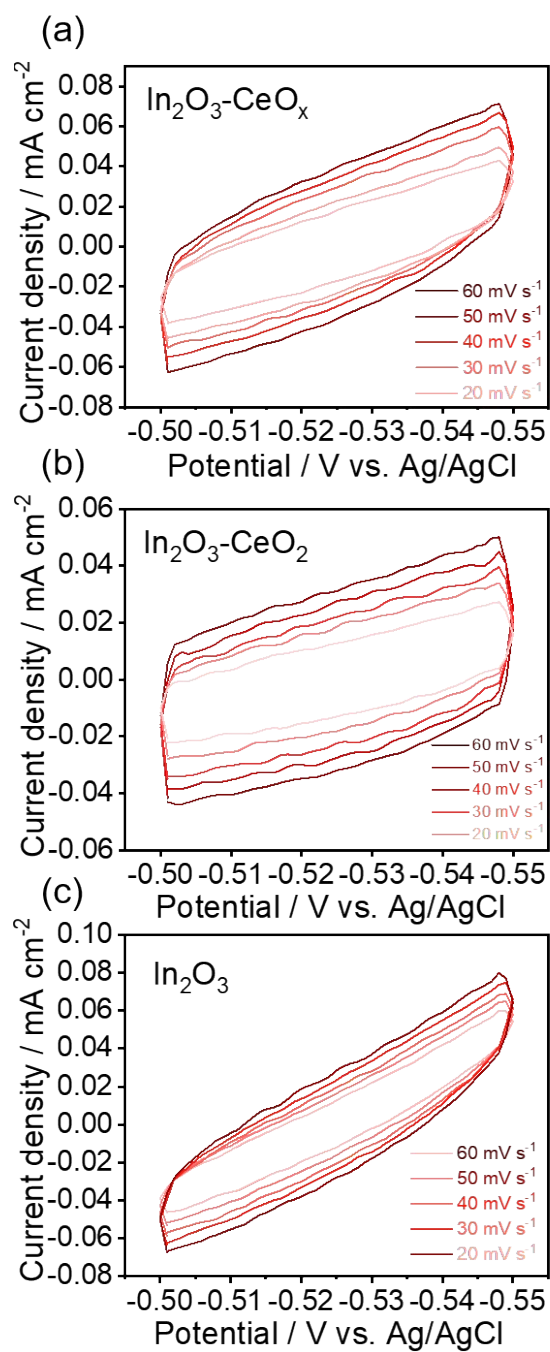


Figure S10. Cyclic voltammograms of a) In₂O₃-CeO_x, b) In₂O₃-CeO₂ and c) In₂O₃ between -0.55V and -0.50 V vs. RHE in CO₂-saturated 0.5 M KHCO₃.

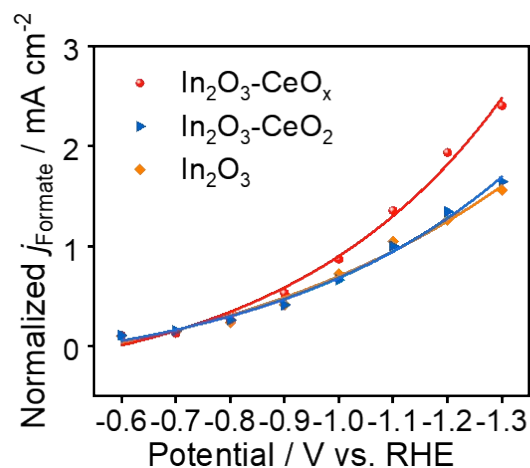


Figure S11. The normalized current density for formate production by ECSA for $\text{In}_2\text{O}_3\text{-CeO}_x$, $\text{In}_2\text{O}_3\text{-CeO}_2$ and In_2O_3 .

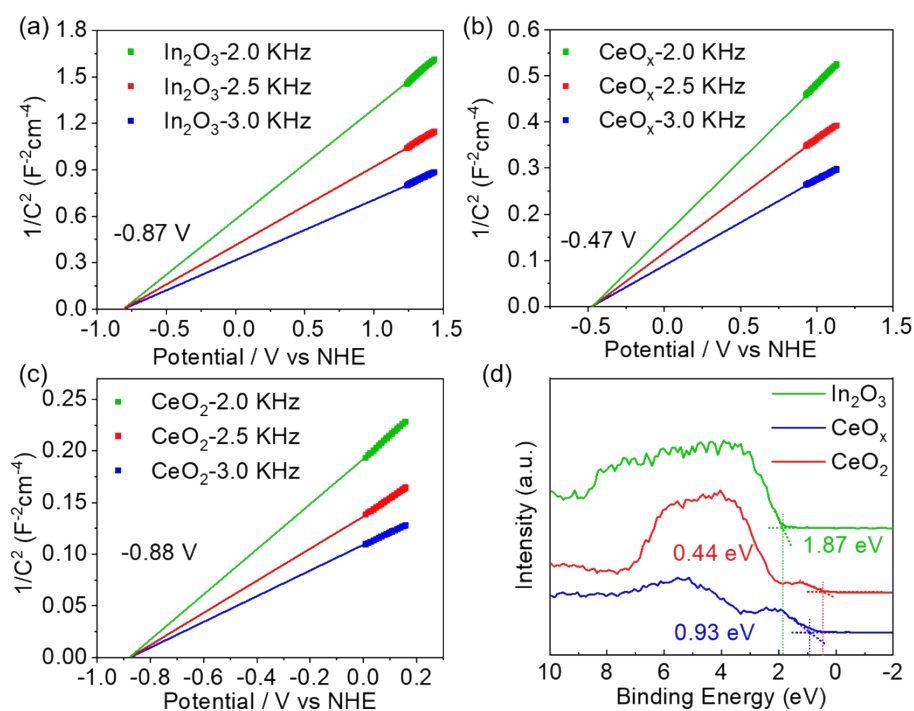


Figure S12. a-c) Mott-Schottky plots of In_2O_3 , CeO_x and CeO_2 respectively. d) valence band XPS spectra.

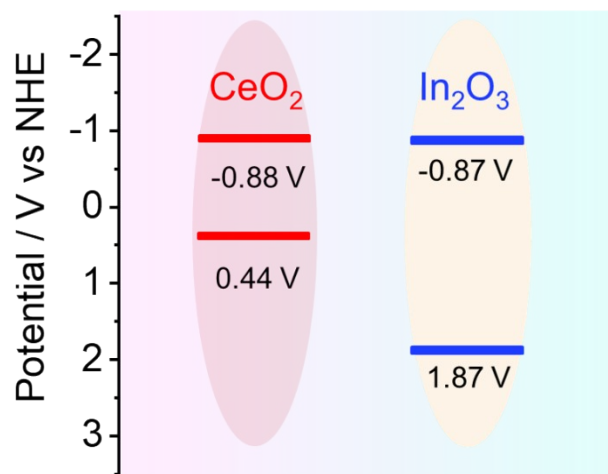


Figure S13. Schematic illustration for charge transfer in $\text{In}_2\text{O}_3\text{-CeO}_2$.

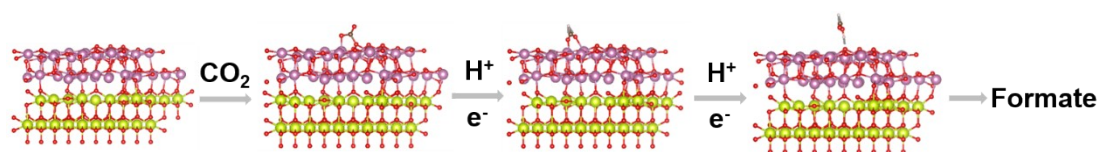


Figure S14. The catalytic pathway on $\text{In}_2\text{O}_3\text{-CeO}_x$ based on the $^*\text{OCHO}$ and $^*\text{HCOOH}$ adsorption intermediates after optimization. Purple, yellow, red, brown, white spheres represent In, Ce, O, C, and H atoms, respectively.

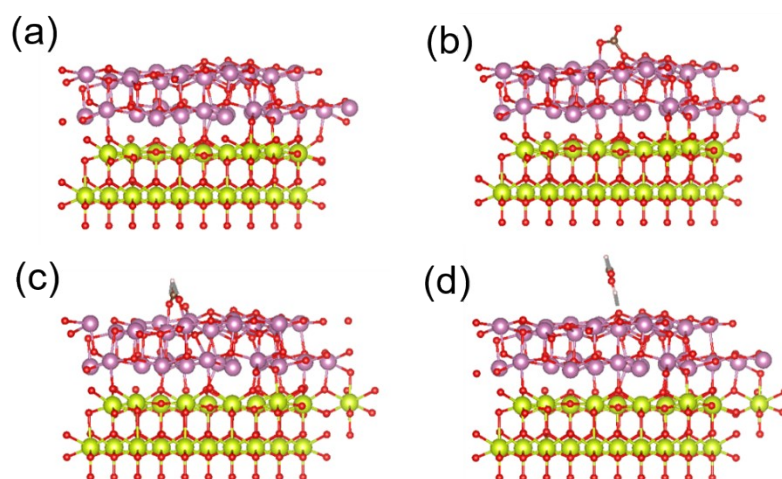


Figure S15. The computational structure and adsorption models In₂O₃-CeO₂ after optimization. a) In₂O₃-CeO₂, b) *CO₂ on In₂O₃-CeO₂, c) *OCHO on In₂O₃-CeO₂, d) *HCOOH on In₂O₃-CeO₂. Purple, yellow, red, brown, white spheres represent In, Ce, O, C, and H atoms, respectively.

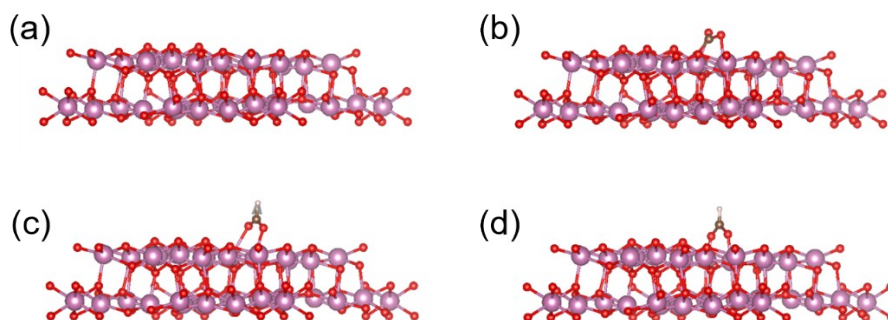


Figure S16. The computational structure and adsorption models In₂O₃ after optimization. a) In₂O₃, b) *CO₂ on In₂O₃, c) *OCHO on In₂O₃, d) *HCOOH on In₂O₃. Purple, yellow, red, brown, white spheres represent In, Ce, O, C, and H atoms, respectively.

Table 1. Comparison of the highest FE and potential on some reported In-based electrocatalysts for the electrochemical reduction of CO₂ to formate.

Catalysts	Max FE _{Formate}	Potential	References
In ₂ O ₃ /InN	95.7%	-1.48 V	[14]
MIL-68(In)-NH ₂	94.4%	-1.1 V	[15]
Ni-In ₂ O ₃ @CNFs	93.6%	-0.8 V	[16]
In/In Oxide	93%	-1.1 V	[17]
H-InO _x NRs	91.7 %	-0.7 V	[18]
In-MOF	90%	-0.9 V	[19]
In/In ₂ O _{3-x}	89.2%	-0.8 V	[20]
In-Co PBA	85%	-0.96 V	[21]
In ₂ O ₃ -rGO	84.6%	-1.2 V	[22]
Sn-InO _x	80%	-1.0 V	[23]
In₂O₃-CeO_x	94.8%	-0.9 V	This Work

References

- (1) Wu, Y.; Chen, C.; Yan, X.; Wu, R.; Liu, S.; Ma, J.; Zhang, J.; Liu, Z.; Xing, X.; Wu, Z.; Han, B., Enhancing CO₂ electroreduction to CH₄ over Cu nanoparticles supported on N-doped carbon. *Chem. Sci.* **2022**, *13*, 8388-8394.
- (2) Yan, X.; Chen, C.; Wu, Y.; Liu, S.; Chen, Y.; Feng, R.; Zhang, J.; Han, B., Efficient electroreduction of CO₂ to C₂₊ products on CeO₂ modified CuO. *Chem. Sci.* **2021**, *12*, 6638-6645.
- (3) Y. Wang; W. Zhou; R. Jia; Y. Yu; B. Zhang. Unveiling the activity origin of a copper-based electrocatalyst for selective nitrate reduction to ammonia. *Angew. Chem. Int. Ed.*, **2020**, *59*, 5350-5354.
- (4) T. D. Kühne; M. Iannuzzi; M. D. Ben; V. V. Rybkin; P. Seewald; F. Stein; T. Laino; R. Z. Khaliullin; O. Schütt; F. Schiffmann; D. Golze; J. Wilhelm; S. Chulkov; M. H. Bani-Hashemian; V. Weber; U. Borštnik; M. Taillefumier; A. S. Jakobovits; A. Lazzaro; H. Pabst; T. Müller; R. Schade; M. Guidon; S. Andermatt; N. Holmberg; G. K. Schenter; A. Hehn; A. Bussy; F. Belleflamme; G. Tabacchi; A. Glöb; M. Lass; I. Bethune; C. J. Mundy; C. Plessl; M. Watkins; J. VandeVondele; M. Krack; J. Hutter. CP2K: An electronic structure and molecular dynamics software package - Quickstep: Efficient and accurate electronic structure calculations. *J. Chem. Phys.*, **2020**, *152*, 194103-194149.
- (5) J. VandeVondele; J. Hutter. Gaussian basis sets for accurate calculations on molecular systems in gas and condensed phases. *J. Chem. Phys.*, **2007**, *127*, 114105-114113.
- (6) S. Goedecker; M. Teter; J. Hutter. Separable dual-space gaussian pseudopotentials. *Phys. Rev. B*, **1996**, *54*, 1703-1710.
- (7) Y.-G. Wang; D. Mei; J. Li; R. Rousseau. DFT+U study on the localized electronic states and their potential role during H₂O dissociation and CO oxidation processes on CeO₂(111) surface. *J. Phys. Chem. C*, **2013**, *117*, 23082-23089.
- (8) K. R. Hahn; M. Iannuzzi; A. P. Seitsonen; J. Hutter. Coverage effect of the CO₂ adsorption mechanisms on CeO₂(111) by first principles analysis. *J. Phys. Chem. C*, **2013**, *117*, 1701-1711.
- (9) S. Grimme; J. Antony; S. Ehrlich; H. Krieg. A consistent and accurate ab initio parametrization of density functional dispersion correction (DFT-D) for the 94 elements H-Pu. *J. Chem. Phys.*, **2010**, *132*, 154104-154123.
- (10) S. Grimme; S. Ehrlich; L. Goerigk. Effect of the damping function in dispersion corrected density functional theory. *J. Comput. Chem.*, **2011**, *32*, 1456-1465.
- (11) T. Lu; Q. Chen. Shermo: A general code for calculating molecular thermochemistry properties. *Comput. Theor. Chem.*, **2021**, *1200*, 113249-113257.
- (12) T. Lu; F. Chen. Multiwfn: A multifunctional wavefunction analyzer. *J Comput Chem*, **2012**, *33*, 580-592.
- (13) P. Ros; A. Van Der Avoird; G. C. A. Schuit. Molecular orbital calculations on copper chloride complexes. *Coord. Chem. Rev.*, **1967**, *2*, 65-75.
- (14) X. Zhao; M. Huang; B. Deng; K. Li; F. Li; F. Dong. Interfacial engineering of In₂O₃/InN heterostructure with promoted charge transfer for highly efficient CO₂ reduction to formate. *Chem. Eng. J.*, **2022**, *437*, 135114-135120.
- (15) Z. Wang; Y. Zhou; C. Xia; W. Guo; B. You; B. Y. Xia. Efficient electroconversion of carbon dioxide to formate by a reconstructed amino-functionalized indium-organic framework electrocatalyst. *Angew. Chem. Int. Ed.*, **2021**, *60*, 19107-19112.
- (16) Z. Chen; G. Yu; B. Li; X. Zhang; M. Jiao; N. Wang; X. Zhang; L. Liu. In situ carbon encapsulation

- confined nickel-doped indium oxide nanocrystals for boosting CO₂ electroreduction to the industrial level. *ACS Catal.*, **2021**, *11*, 14596-14604.
- (17) W. Yang; Y. Zhao; S. Chen; W. Ren; X. Chen; C. Jia; Z. Su; Y. Wang; C. Zhao. Defective indium/indium oxide heterostructures for highly selective carbon dioxide electrocatalysis. *Inorg. Chem.*, **2020**, *59*, 12437-12444.
- (18) J. Zhang; R. Yin; Q. Shao; T. Zhu; X. Huang. Oxygen vacancies in amorphous InO_x nanoribbons enhance CO₂ adsorption and activation for CO₂ electroreduction. *Angew. Chem. Int. Ed.*, **2019**, *58*, 5609-5613.
- (19) B. Pan; G. Yuan; X. Zhao; N. Han; Y. Huang; K. Feng; C. Cheng; J. Zhong; L. Zhang; Y. Wang; Y. Li. Highly dispersed indium oxide nanoparticles supported on carbon nanorods enabling efficient electrochemical CO₂ reduction. *Small Sci.*, **2021**, *1*, 2100029.
- (20) Y. Liang; W. Zhou; Y. Shi; C. Liu; B. Zhang. Unveiling in situ evolved In/In₂O₃-heterostructure as the active phase of In₂O₃ toward efficient electroreduction of CO₂ to formate. *Sci. Bull.*, **2020**, *65*, 1547-1554.
- (21) J. Zhai; Q. Kang; Q. Liu; D. Lai; Q. Lu; F. Gao. In-situ generation of In₂O₃ nanoparticles inside In[Co(CN)₆] quasi-metal-organic-framework nanocubes for efficient electroreduction of CO₂ to formate. *J. Colloid Interface Sci.*, **2022**, *608*, 1942-1950.
- (22) Z. Zhang; F. Ahmad; W. Zhao; W. Yan; W. Zhang; H. Huang; C. Ma; J. Zeng. Enhanced wlectrocatalytic reduction of CO₂ via chemical coupling between indium oxide and reduced graphene oxide. *Nano Lett.*, **2019**, *19*, 4029-4034.
- (23) L. C. Pardo Pérez; D. Teschner; E. Willinger; A. Guiet; M. Driess; P. Strasser; A. Fischer. In situ formed “Sn_{1-x}In_x@In_{1-y}Sn_yO_z” core@shell nanoparticles as electrocatalysts for CO₂ reduction to formate. *Adv. Funct. Mater.*, **2021**, *31*, 2103601.